THE JOURNAL OF PHYSICAL CHEMISTRY Letters

Letter

Cite This: J. Phys. Chem. Lett. 2019, 10, 4252−4258

pubs.acs.org/JPCL

Cavity-Modified Exciton Dynamics in Photosynthetic Units

Rocío Sáez-Blázquez,[†] Johannes Feist,[†] Elisabet Romero,[‡] Antonio I. Fernández-Domínguez,*[,†] and Francisco J. García-Vidal*[,†,§]

[†]Departamento de Física Teórica de la Materia Condensada and Condensed Matter Physics Center (IFIMAC), Universidad Autónoma de Madrid, E-28049 Madrid, Spain

[‡]Institute of Chemical Research of Catalonia (ICIQ), Barcelona Institute of Science and Technology (BIST), E-43007 Tarragona, Spain

[§]Donostia International Physics Center (DIPC), E-20018 Donostia−San Sebastián, Spain

ABSTRACT: Recently, exciton−photon strong coupling has been proposed as a means to control and enhance energy transfer in ensembles of organic molecules. Here, we demonstrate that the exciton dynamics in an archetypal purple bacterial photosynthetic unit, composed of six LH2 antennas surrounding a single LH1 complex, is greatly modified by its interaction with an optical cavity. We develop a Bloch−Redfield master equation approach that accounts for the interplay between the B800 and B850 bacteriochlorophyll molecules within each LH2 antenna, as well as their interactions with the central LH1 complex. Using a realistic parametrization of both the photosynthetic unit and optical cavity, we investigate the formation of polaritons in the system, revealing that these can be tuned to accelerate its exciton dynamics by 3 orders of magnitude. This yields a significant occupation of the LH1 complex, the stage immediately prior to the reaction center, with only a few-femtosecond delay after the initial excitation of the LH2 B800 pigments. Our theoretical findings unveil polaritonic phenomena as a promising route for the characterization, tailoring, and optimization of light-harvesting mechanisms in natural and artificial photosynthetic processes.

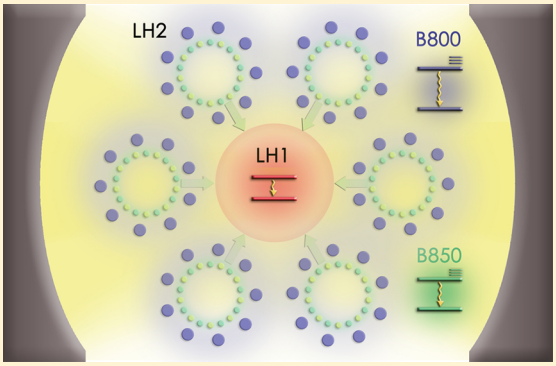

Light-harvesting (LH) complexes play a crucial role in the process of photosynthesis.[1,2] They are responsible for collecting, retaining, and funnelling solar energy[3,4] into the reaction centers, where its conversion into chemical energy takes place.[5] These pigment−protein compounds absorb the incident photons and convey the resulting electron−hole excitations through Förster-like, dipole−dipole interactions between neighboring molecules.[6,7] This mechanism is slower than vibrational dephasing in the system, which makes the transport process effectively incoherent.[8,9] Moreover, thanks to the extremely slow nonradiative decay inherent to bacteriochlorophyll molecules, energy transfer in photosynthetic membranes can range micrometric distances and take nanoseconds while having efficiencies approaching 100%.[10,11] A paradigmatic example of phototrophic organisms, widely studied in the literature, is purple bacteria[12,13] such as *Rhodopseudomonas acidophila*, in whose photosynthetic membranes two different complexes can be identified:[14] LH2, which act mainly as optical antennas, and LH1, which deliver the excitation to the reaction center they enclose. Although the arrangement and distribution of both complexes within the bacterial membrane depend on the ambient and light intensity conditions, there is usually a number of LH2 in the vicinity of every LH1 and attached reaction center.[10,15]

In recent years, much research attention has been focused on exploring the opportunities that the phenomenon of exciton−photon collective strong coupling[16] brings into material science.[17] The coupling between an excitonic platform and the electromagnetic modes supported by an optical cavity gives rise to polaritons, hybrid states whose formation requires that the interaction between light and matter become faster than their respective decay channels. Experimental and theoretical studies demonstrate that the appropriate tailoring of polaritonic characteristics in organic semiconductors and ensembles of organic molecules can yield a large enhancement of the efficiency and spatial range of charge and exciton conductance[18−21] and energy transfer[22−26] in these systems. The coherent and delocalized nature of polaritons plays a crucial role in these phenomena. On one hand, it allows energy transfer within a time scale set by the so-called Rabi frequency (collective coupling strength).[27] On the other hand, it makes the process nonlocal and robust to disorder within a length scale comparable to the optical wavelength.[28]

It has been recently shown that plasmonic nanostructures can modify the optical properties of LH2 antennas.[29−32] Moreover, experimental evidence of collective strong coupling in ensembles of living bacteria has been reported,[33] giving rise

Received: May 24, 2019
Accepted: July 10, 2019
Published: July 10, 2019

DOI: 10.1021/acs.jpclett.9b01495
J. Phys. Chem. Lett. 2019, 10, 4252−4258

even to the concept of *living polaritons*.[34] In ref 33, a Rabi splitting of around 150 meV has been reported, implying that about 1000 chlorosomes present in green sulfur bacteria are coherently coupled to a cavity photon. In the absence of a cavity, the study of exciton transport in photosynthetic materials has been triggered by the prospect of transferring this knowledge to human-made energy-harvesting structures. In this Letter, we go a step further by assessing the impact that the interaction with an optical cavity has on the efficiency of exciton transport taking place in purple bacterial photosynthetic units (PSUs) formed by several LH complexes. Using Bloch–Redfield theory,[35,36] which allows us to describe vibration-assisted incoherent interactions among bacteriochlorophyll pigments,[6,9] we construct first a quantum master equation describing a single LH2 antenna, involving 27 interacting pigments of three different families (B800, B850a, and B850b). Our model reproduces experimental absorption spectra of freestanding LH2. Next, we consider an archetypal PSU configuration:[10,37] a ring of six LH2 antennas surrounding a single LH1 complex. We extend our master equation to the whole PSU, including incoherent interactions among neighboring pigments within different LH complexes. By introducing pigment–photon coupling terms in the Hamiltonian, we study the formation of polaritons in the system, with special emphasis on the cavity characteristics. We find that strong coupling in realistic cavities can accelerate PSU exciton dynamics by a factor $\sim 10^3$, which leads to a considerable population of the LH1 complex within only a few femtoseconds after the initial excitation of LH2 B800 pigments. Our model also reveals how the contribution of the different polaritonic states to this fast population transfer depends on the frequency of the cavity mode and its effective volume (or pigment–photon coupling strength).

Figure 1a sketches the PSU configuration under study: six LH2 antennas arranged around a single LH1 complex. The latter is formed by a number of B875 pigments,[4] which are the final stage of the exciton transfer mechanism we analyze here. Taking this into account, we use a simplified model for the LH1 complex (red circle), valid in the low population regime. We treat it as a single two-level system with transition frequency $\omega_{\mathrm{LH1}} = 1.417$ eV.[38] Our attention is focused on the LH2 antennas, which we describe in more detail. They are composed of $N_{\mathrm{LH2}} = 27$ pigments, distributed in a double-ring structure:[39−41] while nine B800 molecules (blue dots) form one of the rings, the other comprises nine pigment dimers made up of a B850a and a B850b molecule each (light and dark green dots). In our model, the pigments in each LH2 complex are modeled as interacting two-level systems leading to the Hamiltonian

$$\hat{H}_{\mathrm{LH2}} = \sum_{i=1}^{N_{\mathrm{LH2}}} \omega_i \hat{\sigma}_i^{\dagger}\hat{\sigma}_i + \sum_{i,j=1}^{N_{\mathrm{LH2}}} V_{ij}\{\hat{\sigma}_i^{\dagger}\hat{\sigma}_j + \hat{\sigma}_j^{\dagger}\hat{\sigma}_i\} \tag{1}$$

where $\hat{\sigma}_i^{\dagger}$ and $\hat{\sigma}_i$ are the creation and annihilation operators of molecular excitations, and ω_i is their corresponding energies. The parameters in eq 1 are taken from refs 44 and 45. The freestanding-pigment energies are set to $\omega_{\mathrm{B800}} = 1.549$ eV and $\omega_{\mathrm{B850a,b}} = 1.520$ eV. The intraring nearest-neighbor (second-nearest-neighbor) couplings are $V_{\mathrm{B800B800}} = 3$ meV, $V_{\mathrm{B850aB850a}} = 6$ meV, $V_{\mathrm{B850bB850b}} = 4$ meV, and $V_{\mathrm{B850aB850b}} = -33(-36)$ meV. Finally, the inter-ring nearest-neighbor interaction is parametrized by $V_{\mathrm{B800B850a}} = -3$ meV and $V_{\mathrm{B800B850b}} = -1$ meV.

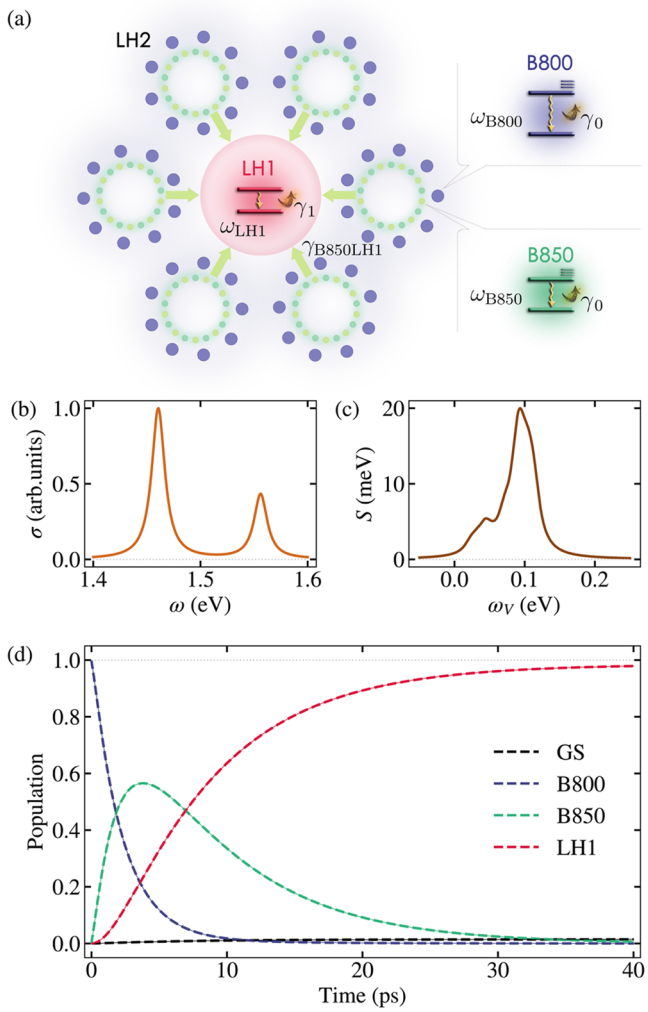

Figure 1. (a) Sketch of the PSU considered in this work: 6 LH2 antennas, comprising 9 B800 and 18 B850 molecules each, surrounding a single LH1 complex. The insets show the two-level system exciton model of B-molecules and LH1, which experience both radiative and vibrational decay. (b) Absorption spectrum of a single LH2 complex, including disorder and inhomogeneous broadening. (c) Vibrational spectral density, $S(\omega)$, for all LH2 pigments. (d) Exciton population dynamics for the PSU in panel a in an initial state given by the superposition of excited B800 molecules in the six LH2 antennas.

The diagonalization of the Hamiltonian above yields the exciton energies of the LH2 complex. The small inter-ring couplings above translate into excitons strongly localized at B800 or B850(a,b) pigments, with little hybridization among them.[40,41] We check the validity of our model by calculating the absorption spectrum for a single, isolated LH2 antenna. We first compute the transition matrix element of the total dipole moment operator $\hat{M} = \sum_{i=1}^{N_{\mathrm{LH2}}} \mu_i \hat{\sigma}_i^{\dagger}$ ($\mu_{\mathrm{B800}} = \mu_{\mathrm{B850}} = 6.13$ D[46]) for the excitonic eigenstates of eq 1. The absorption spectrum is built as a sum of Lorentzian contributions centered at the excitonic energies and weighted by the square of the corresponding matrix element of the dipole moment operator. Their width was set to 15 meV for B800 and B850 excitons, to take into account the disorder and inhomogeneous broadening inherent to the measurements performed on ensembles of LH2 complexes.[47] The spectrum obtained this way is rendered in Figure 1b, which reproduces the double-peaked absorption

DOI: 10.1021/acs.jpclett.9b01495
J. Phys. Chem. Lett. 2019, 10, 4252−4258

profile reported experimentally,[47,48] with maxima around 1.44 eV (860 nm) and 1.55 eV (800 nm).

We use a Bloch−Redfield master equation[6] to describe the vibrational dissipation and incoherent interactions experienced by B800 and B850 molecules. This requires the inclusion of the vibronic spectral density of the pigments, $S(\omega)$. Figure 1c plots $S(\omega)$ in our calculations (the same for B800 and B850 molecules), parametrized using the Franck−Condon factors in ref 42 and a thermal line broadening in agreement with ref 43. Lindblad terms of the form $\frac{\gamma_0}{2}\mathcal{L}_{\hat{\sigma}_i}[\hat{\rho}] = \frac{\gamma_0}{2}[2\hat{\sigma}_i\hat{\rho}\hat{\sigma}_i^{\dagger} - \{\rho\hat{\sigma}_i^{\dagger}\hat{\sigma}_i\}]$, acting on all pigment annihilation operators, are also included in the master equation, weighted by a decay rate $\gamma_0 = 1$ μeV, which reflects the ∼1 ns lifetime of all the molecules in the LH2 complex.[4] Note that the exciton widths introduced in the cross-section calculations are $\sim 10^4$ times larger than this value.

The master equation for the whole PSU is built next. It is composed by blocks, corresponding to the six LH2 antennas and the central LH1 complex, only connected through Lindblad terms of the form $\frac{\gamma_{B850LH1}}{2}\mathcal{L}_{\hat{\sigma}_{LH1}^{\dagger}\hat{\sigma}_{n,1}}[\hat{\rho}]$. These act on the product of the annihilation operator for the B850 molecule (which we label as $i = 1$) in the nth LH2 antenna that is located next to the LH1 complex, and the LH1 creation operator. The associated decay rate is set to $\gamma_{B850LH1} = 2$ meV, which yields LH2−LH1 transition rates in agreement with experiments.[37] This is shown in Figure 1d, which plots the population transients for a freestanding PSU. The initial state corresponds to the coherent superposition of excitations in all the B800 pigments, which mimics an experimental setup in which the PSU is pumped by an ultrashort laser pulse centered around 800 nm. We can observe that this state (blue line) decays within ∼3 ps, feeding population into the LH2 B850 molecules (green line). These in turn carry the excitation to the LH1 complex (red line), whose population grows within a ∼20 ps time scale after the initial excitation. The time interval in Figure 1d is much shorter than γ_0^{-1}, and the ground state (shown in black line) is negligibly populated in the whole exciton transfer process. Note that we have taken $\gamma_1 = 0$, see Figure 1a, to avoid the decay of the LH1 excitations into the ground state.

To analyze the effect of strong coupling in the PSU exciton dynamics, we add new terms to the freestanding PSU Hamiltonian, describing the coherent interactions between pigments and cavity photons

$$\hat{H} = \omega_C\hat{a}^{\dagger}\hat{a} + \omega_{LH1}\hat{\sigma}_{LH1}^{\dagger}\hat{\sigma}_{LH1} + \sum_{n=1}^{6}\hat{H}_{LH2,n} + g_0\left[\sum_{n=1}^{6}\sum_{i=1}^{N_{LH2}}(\hat{\sigma}_{n,i}^{\dagger}\hat{a} + \hat{\sigma}_{n,i}\hat{a}^{\dagger}) + \eta(\hat{\sigma}_{LH1}^{\dagger}\hat{a} + \hat{\sigma}_{LH1}\hat{a}^{\dagger})\right] \quad (2)$$

where ω_C is the cavity frequency, $\hat{a}^{\dagger}$ and $\hat{a}$ are the creation and annihilation operators for the cavity mode, g_0 is the photon coupling strength to all LH2 pigments, and $\eta = 3.8$ is the dipole moment of the LH1 complex normalized to μ_{B800}.[4] There, $\hat{H}_{LH2,n}$ is the Hamiltonian for the nth LH2 antenna (see eq 1). As a result of the interaction between molecules and cavity and the symmetry of the structure, only four hybrid light−matter states arise when entering into the strong-coupling regime, in addition to the set of the so-called dark states. These states are linear combinations of electronic excitations within the LH1 and LH2 complexes that do not couple to the cavity mode. Figure 2a renders the four polaritonic frequencies, as well as those corresponding to the

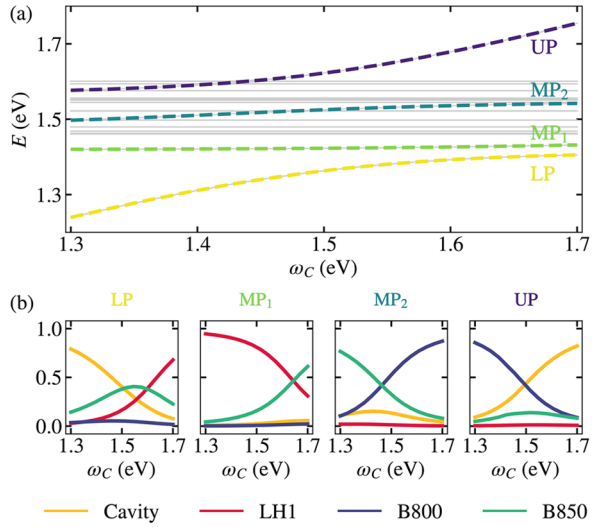

Figure 2. (a) Energies of the lower (LP, yellow), middle (MP_1, green, and MP_2, blue), and upper (UP, violet) polaritons versus the cavity frequency, ω_C, and for $g_0 = 9$ meV. (b) Coefficients representing the cavity (yellow), LH1 (red), B800 (blue), and B850 (green) content of the four polaritons in panel a as a function of ω_C.

set of dark states, versus the cavity frequency. They are obtained directly from the diagonalization of eq 2. Color lines plot the dispersion of the lower (LP, yellow), middle (MP_1 and MP_2, green and blue), and upper (UP, violet) polariton bands. Note that, certainly, the PSU dark states (gray lines) remain uncoupled to the cavity field. In our calculations, we have taken $g_0 = 9$ meV. Using $g_0 = \mu_{B800}\sqrt{\omega_C/2\epsilon_0 V_{eff}}$,[49] this value corresponds to $V_{eff} = (15\text{ nm})^3$ at $\omega_C = 1.6$ eV. This is attainable not only in plasmonic but also in state-of-the-art dielectric cavities.[50]

Figure 2b shows, from left to right, the square of the Hopfield coefficients for the LP, MP_1, MP_2, and UP as a function of the cavity frequency. Calculated as $|\langle i|\alpha\rangle|^2$, where $\alpha(i)$ labels the polaritonic (exciton and cavity) states, they weight the cavity (yellow), LH1 (red), B800 (blue), and B850 (green) contents of each polariton. We can observe that the polariton character can be greatly modified through ω_C. Note that only the LP and UP present a substantial cavity content, but they do it at low and high cavity frequencies, respectively. Far from these spectral regions, LP (UP) virtually overlaps with the LH1 (B800) states. On the contrary, the MPs present a moderate cavity component but combine excitonic contents corresponding to all PSU pigments. We anticipate that the hybrid character of these states (especially evident for MP_2 at $\omega_C \simeq 1.45$ eV, where B800 and B850 coefficients become similar) will play a fundamental role in the polariton-assisted population transfer in the PSU.[26]

Having studied the formation of polaritons in the hybrid cavity−PSU system, and the tuning of their characteristics through the cavity frequency, we investigate next its population dynamics. To do so, we extend the master equation for the freestanding PSU by the inclusion of the Hamiltonian in eq 2, and by adding a Lindblad term describing the cavity losses. We set the cavity decay rate to $\gamma_C = 13$ μeV, which corresponds to a lifetime of 50 ps and a quality factor $Q = \omega_C/2\gamma_C \simeq 6 \times 10^4$,

DOI: 10.1021/acs.jpclett.9b01495
J. Phys. Chem. Lett. 2019, 10, 4252−4258

parameters similar to those recently reported in deeply subwavelength dielectric cavities.[50] Similarly to Figure 1d and to perform a meaningful comparison against the freestanding PSU, we set the initial state as the coherent superposition of equally excited B800 molecules, and choose ω_C = 1.6 eV and g_0 = 9 meV. Figure 2b shows that the LP is composed of LH1 excitations mostly at this cavity frequency, which allows us to set the final stage of the polariton-assisted energy transfer mechanism at the LH1 complex.

Figure 3 displays the comparison between the population dynamics for the PSU in isolation (dashed lines) and

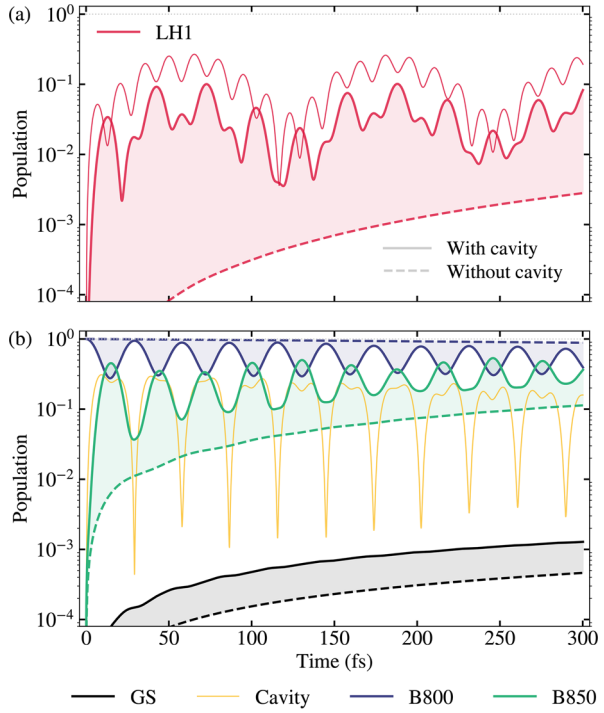

Figure 3. Exciton dynamics for the PSU in Figure 1. (a) LH1 population versus time after the initial excitation of the B800 molecules for the PSU isolated (dashed line) and coupled to an optical cavity with ω_C = 1.6 eV and g_0 = 9 meV (solid line). The thin solid line plots the LH1 population for an initial excitation of the cavity mode. (b) Temporal evolution of the ground state (black), B800 (blue), and B850 (green) populations with (solid line) and without (dashed line) cavity. The cavity population is shown in the yellow solid line. The differences between populations have been shaded in all cases to highlight the effect of strong coupling.

interacting with the cavity described above (solid lines). Figure 3a shows that exciton−photon strong coupling in the PSU gives rise to an extremely fast occupation of the LH1 complex, which acquires a significant population (∼10%) within only a 20 fs delay. In absence of the cavity, the LH1 population is negligible in this time scale and becomes comparable only after a few ps (see Figure 1d). This is the main result in this Letter, the polariton-assisted reduction in population transfer times taking place in PSUs by 3 orders of magnitude. The thin solid line renders the LH1 population when the cavity, instead of the B800 pigments, is initially excited, proving that this phenomenon also takes place in this configuration.

Figure 3b plots the population transients for B800 (blue) and B850 (green) excitons, both exhibiting more regular Rabi oscillations than the LH1. These are especially apparent in the B800 case. Its occupation remains constant and close to unity for the freestanding PSU, but the occurrence of strong coupling gives rise to a coherent energy exchange that feeds population into the other excitonic and cavity (yellow line) states. Black lines correspond to the ground state, whose population is larger in the strong-coupling regime. This is a consequence of the short lifetime of the cavity relative to the PSU pigments ($\gamma_C \sim \gamma_0/20$). This loss channel can be mitigated by using nanocavities with higher-quality factors. Note that all the time traces in Figure 3 were calculated assuming the same coupling strength for all the B800 and B850 pigments in the PSU (see eq 2). Importantly, our findings hold beyond this approximation, as long as the PSU−cavity Rabi frequency remains the same as in the uniform description.[26]

Up to this point, we have demonstrated that the exciton dynamics in PSUs is greatly modified due to the interaction with a particular optical cavity configuration. We have also shown that this phenomenon is mediated by the polaritons that emerge in the system, whose character varies strongly with the frequency of the cavity. In the following, we shed insights into both findings by investigating the dependence of the B800-to-LH1 population transfer and the polaritonic content of B800 and LH1 excitations on the two parameters set by the optical cavity: ω_C and g_0. Figure 4a displays a contour plot of the LH1 population averaged over the first 300 fs after the excitation of the B800 molecules (the time span in Figure 3). Note that the temporal averaging naturally removes peak effects related to the irregular Rabi oscillations apparent in Figure 3a. We can observe that, by increasing the exciton−photon coupling (reducing the cavity mode volume), the LH1 population grows, although not in a purely monotonic fashion (small oscillations are apparent). On the contrary, the dependence on ω_C is much weaker. This is a surprising result, given the strong dependence of the Hopfield coefficients, and therefore the polariton character, on the cavity frequency shown in Figure 2b.

Figure 4b plots the combination of content of B800 and LH1 excitations on the various polaritons α, $\chi_\alpha = |\langle\alpha|\mathrm{LH1}\rangle|^2 |\langle\alpha|\mathrm{B800}\rangle|^2$, as a function of the cavity frequency and coupling strength. We can observe that, as expected, χ_α grows with g_0 in all cases, as the light−matter hybridization increases with this parameter. However, the B800 and LH1 projections over the different polaritons vary much with ω_C. For large couplings (g_0 > 10 meV), χ_{LP} dominates LH1 excitations for blue-detuned cavities, whereas χ_{MP_2} and χ_{UP} are the largest contributions for red-detuned ones. On the other hand, for modest couplings ($g_0 \lesssim$ 10 meV), χ_{LP} and χ_{MP_1} are largest for red-detuned cavities, while χ_{MP_2} and χ_{UP} present a maximum within the spectral window between 1.5 and 1.6 eV. These panels indicate that the interplay among the different polaritons plays a crucial role in the fast B800-to-LH1 population transfer in PSUs. This conclusion is supported by the contour lines in Figure 4a, which render $\sum_\alpha \chi_\alpha$, showing that this magnitude presents the same dependence on ω_C and g_0 as the LH1 averaged population.

Finally, Figure 4c displays the LH1 population evaluated 40 ps after the initial B800 excitation. We can observe that, for the cavity parameters in Figure 3 (which maximize its population at short times), the LH1 occupation at long times is ∼50%, lower than for the freestanding PSU (see Figure 1d). The origin of this low LH1 occupation at long times can be found in Figure 2b. Note that the Hopfield coefficients for the LP

DOI: 10.1021/acs.jpclett.9b01495
J. Phys. Chem. Lett. 2019, 10, 4252−4258

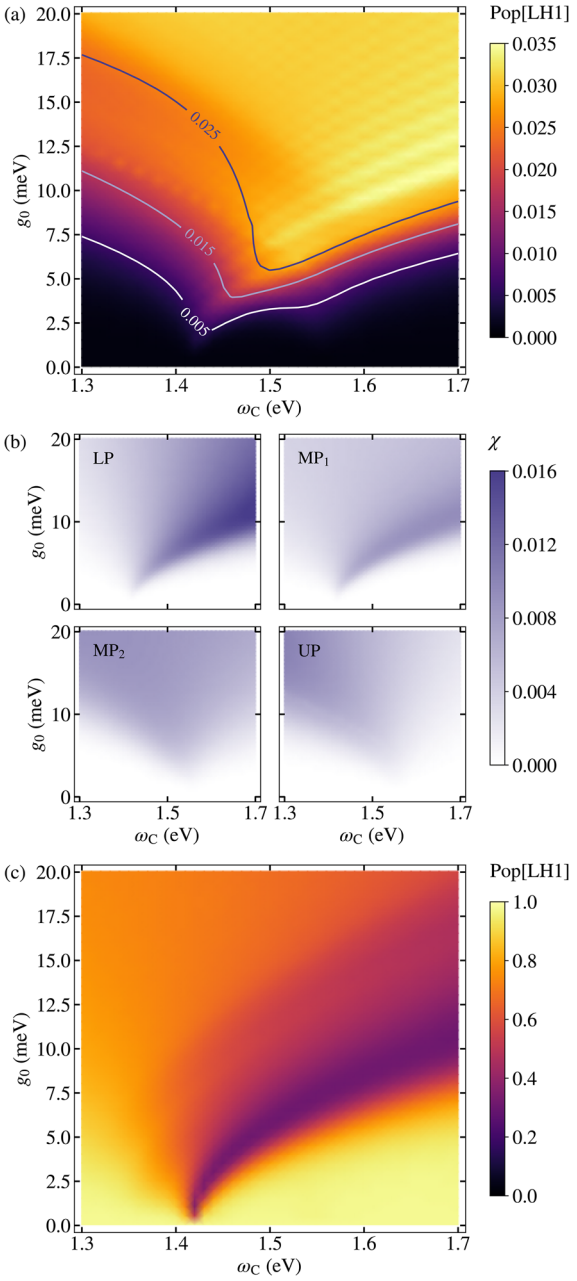

Figure 4. (a) LH1 population averaged over the first 300 fs after the excitation of the LH2 B800 pigments versus cavity frequency and photon−exciton coupling strength. Color solid lines render contours of the magnitude $\sum_\alpha \chi_\alpha$ (see panel below). (b) Polariton component of B800 and LH1 excitations, $\chi_\alpha = |\langle\alpha|\text{LH1}\rangle|^2\ |\langle\alpha|\text{B800}\rangle|^2$, with α = LP, MP_1, MP_2, and UP. (c) LH1 population 40 ps after the initial excitation of the system as a function of ω_C and g_0.

reveal that the lowest energy level in the hybrid PSU−cavity system has only a 50% content on the LH1 state at ω_C = 1.6 eV. However, the comparison between Figures 4a and 4c proves that a compromise between populations at short and long times can be achieved at large coupling strengths (g_0 > 10 meV) and intermediate cavity frequencies ($\omega_C \simeq$ 1.5 eV).

To conclude, we have investigated exciton−photon strong coupling in an archetypal purple bacterial photosynthetic unit, comprising six LH2 antennas surrounding a single LH1 complex. We have developed a master equation combining Bloch−Redfield and Lindblad approaches to describe the vibration-assisted incoherent interactions among the B800, B850, and LH1 excitons, as well as their coherent coupling to the electromagnetic mode supported by an optical cavity. Using this tool, we have explored the formation of polaritons in the system, analyzing their dependence on the cavity configuration. We have revealed that these hybrid light−matter states yield a 3 orders of magnitude reduction in the B800-to-LH1 population transfer times, leading to a significant LH1 occupation in a few-femtosecond time scale. We believe that our theoretical findings demonstrate the potential of exciton−photon strong coupling not only for the characterization of light-harvesting phenomena in natural photosynthesis but also as a means for the design and optimization of artificial photosynthetic systems.

AUTHOR INFORMATION

Corresponding Authors

*E-mail: a.fernandez-dominguez@uam.es.
*E-mail: fj.garcia@uam.es.

ORCID

Johannes Feist: 0000-0002-7972-0646
Antonio I. Fernández-Domínguez: 0000-0002-8082-395X
Francisco J. García-Vidal: 0000-0003-4354-0982

Notes

The authors declare no competing financial interest.

ACKNOWLEDGMENTS

This work has been funded by the European Research Council under Grant Agreements ERC-2011-AdG 290981 and ERC-2016-STG-714870, the EU Seventh Framework Programme (FP7-PEOPLE-2013-CIG-630996), and the Spanish MINECO under contracts MAT2014-53432-C5-5-R and FIS2015-64951-R, and through the "María de Maeztu" programme for Units of Excellence in R&D (MDM-2014-0377), as well as through two Ramon y Cajal grants (J.F. and A.I.F.-D.). We also acknowledge support by the QuantERA program of the European Commission with funding by the Spanish AEI through project PCI2018-093145. E.R. thanks the ICIQ Foundation for the Starting Career Programme and the Generalitat de Catalunya for the CERCA Programme.

REFERENCES

(1) Scholes, G. D.; Fleming, G. R.; Olaya-Castro, A.; van Grondelle, R. Lessons from nature about solar light harvesting. *Nat. Chem.* **2011**, *3*, 763−774.
(2) Croce, R.; van Amerongen, H. Natural strategies for photosynthetic light harvesting. *Nat. Chem. Biol.* **2014**, *10*, 492−501.
(3) McConnell, I.; Li, G.; Brudvig, L. G. Energy conversion in natural and artificial photosynthesis. *Chem. Biol.* **2010**, *17*, 434−47.
(4) Mirkovic, T.; Ostroumov, E.; Anna, J. M.; van Grondelle, R.; Govindjee; Scholes, G. D. Light absorption and energy transfer in the antenna complexes of photosynthetic organisms. *Chem. Rev.* **2017**, *117*, 249−293.
(5) Romero, E.; Novoderezhkin, V. I.; van Grondelle, R. Quantum design of photosynthesis for bio-inspired solar-energy conversion. *Nature* **2017**, *543*, 355−365.
(6) Novoderezhkin, V. I.; van Grondelle, R. Physical origins and models of energy transfer in photosynthetic light-harvesting. *Phys. Chem. Chem. Phys.* **2010**, *12*, 7352−7365.
(7) Ye, J.; Sun, K.; Zhao, Y.; Yu, Y.; Lee, C. K.; Cao, J. Excitonic energy transfer in light-harvesting complexes in purple bacteria. *J. Chem. Phys.* **2012**, *136*, 245104.
(8) Cheng, Y.-C.; Fleming, G. R. Dynamics of light harvesting in photosynthesis. *Annu. Rev. Phys. Chem.* **2009**, *60*, 241−62.

DOI: 10.1021/acs.jpclett.9b01495
J. Phys. Chem. Lett. 2019, 10, 4252−4258

(9) Fassioli, F.; Dinshaw, R.; Arpin, P. C.; Scholes, G. D. Photosynthetic light harvesting: excitons and coherence. *J. R. Soc., Interface* **2014**, *11*, 20130901.
(10) Caycedo-Soler, F.; Rodríguez, F. J.; Quiroga, L.; Johnson, N. F. Light-harvesting mechanism of bacteria exploits a critical interplay between the dynamics of transport and trapping. *Phys. Rev. Lett.* **2010**, *104*, 158302.
(11) Timpmann, K.; Chenchiliyan, M.; Jalviste, E.; Timney, J. A.; Hunter, C. N.; Freiberg, A. Efficiency of light harvesting in a photosynthetic bacterium adapted to different levels of light. *Biochim. Biophys. Acta, Bioenerg.* **2014**, *1837*, 1835−1846.
(12) Hunter, C. N.; Daldal, F.; Thurnauer, M. C.; Beatty, J. T. *The purple phototrophic bacteria*; Springer: Netherlands, 2009.
(13) Cogdell, R. J.; Gall, A.; Köhler, J. The architecture and function of the light-harvesting apparatus of purple bacteria: from single molecules to in vivomembrane. *Q. Rev. Biophys.* **2006**, *39*, 227−324.
(14) Nagarajan, V.; Parson, W. W. Excitation energy transfer between the B850 and B875 antenna complexes of *Rhodobacter Sphaeroides*. *Biochemistry* **1997**, *36*, 2300−2306.
(15) Cleary, L.; Chen, H.; Chuang, C.; Silbey, R. J.; Cao, J. Optimal fold symmetry of LH2 rings on a photosynthetic membrane. *Proc. Natl. Acad. Sci. U. S. A.* **2013**, *110*, 8537−8542.
(16) Lidzey, D. G.; Bradley, D. D. C.; Skolnick, M. S.; Virgili, T.; Walker, S.; Whittaker, D. M. Strong exciton−photon coupling in an organic semiconductor microcavity. *Nature* **1998**, *395*, 53−55.
(17) Ebbesen, T. W. Hybrid light-matter states in molecular and material science. *Acc. Chem. Res.* **2016**, *49*, 2403−2412.
(18) Orgiu, E.; George, J.; Hutchison, J. A.; Devaux, E.; Dayen, J. F.; Doudin, B.; Stellacci, F.; Genet, C.; Schachenmayer, J.; Genes, C.; Pupillo, G.; Samori, P.; Ebbesen, T. W. Conductivity in organic semiconductors hybridized with the vacuum field. *Nat. Mater.* **2015**, *14*, 1123−1129.
(19) Feist, J.; García-Vidal, F. J. Extraordinary exciton conductance induced by strong coupling. *Phys. Rev. Lett.* **2015**, *114*, 196402.
(20) Schachenmayer, J.; Genes, C.; Tignone, E.; Pupillo, G. Cavity-enhanced transport of excitons. *Phys. Rev. Lett.* **2015**, *114*, 196403.
(21) Schlawin, F.; Cavalleri, A.; Jaksch, D. Cavity-mediated electron-photon superconductivity. *Phys. Rev. Lett.* **2019**, *122*, 133602.
(22) Coles, D. M.; Somaschi, N.; Michetti, P.; Clark, C.; Lagoudakis, P. G.; Savvidis, P. G.; Lidzey, D. G. Polariton-mediated energy transfer between organic dyes in a strongly coupled optical microcavity. *Nat. Mater.* **2014**, *13*, 712−719.
(23) Zhong, X.; Chervy, T.; Wang, S.; George, J.; Thomas, A.; Hutchison, J. A.; Devaux, E.; Genet, C.; Ebbesen, T. W. Non-radiative energy transfer mediated by hybrid light-matter states. *Angew. Chem., Int. Ed.* **2016**, *55*, 6202.
(24) Zhong, X.; Chervy, T.; Zhang, L.; Thomas, A.; George, J.; Genet, C.; Hutchison, J. A.; Ebbesen, T. W. Energy transfer between spatially separated entangled molecules. *Angew. Chem., Int. Ed.* **2017**, *56*, 9034.
(25) Du, M.; Martínez-Martínez, M. A.; Ribeiro, R. F.; Hu, Z.; Menon, V. M.; Yuen-Zhou, J. Theory for polariton-assisted remote energy transfer. *Chem. Sci.* **2018**, *9*, 6659−6669.
(26) Sáez-Blázquez, R.; Feist, J.; Fernández-Domínguez, A. I.; García-Vidal, F. J. Organic polaritons enable local vibrations to drive long-range energy transfer. *Phys. Rev. B: Condens. Matter Mater. Phys.* **2018**, *97*, 241407R.
(27) Gonzalez-Ballestero, C.; Feist, J.; Moreno, E.; Garcia-Vidal, F. J. Harvesting excitons through plasmonic strong coupling. *Phys. Rev. B: Condens. Matter Mater. Phys.* **2015**, *92*, 121402R.
(28) García-Vidal, F. J.; Feist, J. Long-distance operator for energy transfer. *Science* **2017**, *357*, 1357−1358.
(29) Wientjes, E.; Renger, J.; Curto, A. G.; Cogdell, R.; van Hulst, N. F. Strong antenna-enhanced fluorescence of a single light-harvesting complex shows photon antibunching. *Nat. Commun.* **2014**, *5*, 4236.
(30) Wientjes, E.; Renger, J.; Cogdell, R.; van Hulst, N. F. Pushing the photon limit: nanoantennas increase maximal photon stream and total photon number. *J. Phys. Chem. Lett.* **2016**, *7*, 1604−1609.
(31) Tsargorodska, A.; Cartron, M. L.; Vasilev, C.; Kodali, G.; Mass, O. A.; Baumberg, J. J.; Dutton, P. L.; Hunter, C. N.; Törmä, P.; Leggett, G. J. Strong coupling of localized surface plasmons to excitons in light-harvesting complexes. *Nano Lett.* **2016**, *16*, 6850−6856.
(32) Caprasecca, S.; Corni, S.; Mennucci, B. Shaping excitons in light-harvesting proteins through nanoplasmonics. *Chem. Sci.* **2018**, *9*, 6219−6227.
(33) Coles, D. M.; Yang, Y.; Wang, Y.; Grant, R. T.; Taylor, R. A.; Saikin, S. K.; Aspuru-Guzik, A.; Lidzey, D. G.; Tang, J. K.-H.; Smith, J. M. Strong coupling between chlorosomes of photosynthetic bacteria and a confined optical cavity mode. *Nat. Commun.* **2014**, *5*, 5561.
(34) Coles, D.; Flatten, L. C.; Sydney, T.; Hounslow, E.; Saikin, S. K.; Aspuru-Guzik, A.; Vedral, V.; Tang, J. K. H.; Taylor, R. A.; Smith, J. M.; Lidzey, D. G. A nanophotonic structure containing living photosynthetic bacteria. *Small* **2017**, *13*, 1701777.
(35) Bloch, F. Generalized theory of relaxation. *Phys. Rev.* **1957**, *105*, 1206.
(36) Redfield, A. G. On the theory of relaxation processes. *IBM J. Res. Dev.* **1957**, *1*, 19.
(37) Ritz, T.; Park, S.; Schulten, K. Kinetics of excitation migration and trapping in the photosynthetic unit of purple bacteria. *J. Phys. Chem. B* **2001**, *105*, 8259−8267.
(38) Caycedo-Soler, F.; Schroeder, C. A.; Autenrieth, C.; Pick, A.; Ghosh, R.; Huelga, S. F.; Plenio, M. B. Quantum redirection of antenna absorption to photosynthetic reaction centers. *J. Phys. Chem. Lett.* **2017**, *8*, 6015−6021.
(39) McDermott, G.; Prince, S. M.; Freer, A. A.; Hawthornthwaite-Lawless, A. M.; Papiz, M. Z.; Cogdell, R. J.; Isaacs, N. W. Crystal structure of an integral membrane light-harvesting complex from photosynthetic bacteria. *Nature* **1995**, *374*, 517−521.
(40) Cupellini, L.; Jurinovich, S.; Campetella, M.; Caprasecca, S.; Guido, C. A.; Kelly, S. M.; Gardiner, A. T.; Cogdell, R.; Mennucci, B. An ab initio description of the excitonic properties of LH2 and their temperature dependence. *J. Phys. Chem. B* **2016**, *120*, 11348−11359.
(41) Caycedo-Soler, F.; Lim, F.; Oviedo-Casado, S.; van Hulst, N. F.; Huelga, S. F.; Plenio, M. B. Theory of excitonic delocalization for robust vibronic dynamics in LH2. *J. Phys. Chem. Lett.* **2018**, *9*, 3446−3453.
(42) Zazubovich, V.; Tibe, I.; Small, G. J. Bacteriochlorophyll a Franck-Condon Factors for the S0→S1(Qy) Transition. *J. Phys. Chem. B* **2001**, *105*, 12410−12417.
(43) De Caro, C.; Visschers, R. W.; van Grondelle, R.; Völker, S. Inter- and intraband energy transfer in LH2-antenna complexes of purple bacteria. A fluorescence line-narrowing and hole-burning study. *J. Phys. Chem.* **1994**, *98*, 10584−10590.
(44) Sauer, K.; Cogdell, R. J.; Prince, S. M.; Freer, A.; Isaacs, N. W.; Scheer, H. Structure-based calculations of the optical spectra of the LH2 bacteriochlorophyll-protein complex from Rhodopseudomonas acidophila. *Photochem. Photobiol.* **1996**, *64*, 564−576.
(45) Tretiak, S.; Middleton, C.; Chernyak, V.; Mukamel, S. Bacteriochlorophyll and carotenoid excitonic couplings in the LH2 system of purple bacteria. *J. Phys. Chem. B* **2000**, *104*, 9540−9553.
(46) Linnanto, J.; Korppi-Tommola, J. E. I.; Helenius, V. M. Electronic States, Absorption spectrum and circular dichroism spectrum of the photosynthetic bacterial LH2 antenna of Rhodopseudomonas acidophilas predicted by exciton theory and semi-empirical calculations. *J. Phys. Chem. B* **1999**, *103*, 8739−8750.
(47) van Oijen, A. M.; Ketelaars, M.; Köhler, J.; Aartsma, T. J.; Schmidt, J. Unraveling the electronic structure of individual photosynthetic pigment-protein complexes. *Science* **1999**, *285*, 400−402.
(48) Hildner, R.; Brinks, D.; Nieder, J. B.; Cogdell, R. J.; van Hulst, N. F. Quantum coherent energy transfer over varying pathways in single light-harvesting complexes. *Science* **2013**, *340*, 1448−1451.
(49) Giannini, V.; Fernández-Domínguez, A. I.; Heck, S. C.; Maier, S. A. Plasmonic nanoantennas: fundamentals and their use in controlling the radiative properties of nanoemitters. *Chem. Rev.* **2011**, *111*, 3888−3912.

DOI: 10.1021/acs.jpclett.9b01495
J. Phys. Chem. Lett. 2019, 10, 4252−4258

(50) Hu, S.; Khater, M.; Salas-Montiel, R.; Kratschmer, E.; Engelmann, S.; Green, W. M. J.; Weiss, S. M. Experimental realization of deep-subwavelength confinement in dielectric optical resonators. *Sci. Adv.* **2018**, *4*, No. eaat2355.

DOI: 10.1021/acs.jpclett.9b01495
J. Phys. Chem. Lett. 2019, 10, 4252−4258